Over-the-Air Calibration of Active Antenna Arrays Using Multisine

Marina Jordão, *Graduate Student Member, IEEE*, Daniel Belo, *Member, IEEE*, Rafael F. S. Caldeirinha, *Senior Member, IEEE*, Arnaldo S. R. Oliveira, *Member, IEEE*, and Nuno Borges de Carvalho, *Fellow, IEEE*

***Abstract*— A novel over-the-air (OTA) beamforming calibration procedure is proposed, which can be applied to different types of multiple-input multiple-output (MIMO) transmitting antennas. The method consists of using two tones on each antenna element, the main tone, and the tickle tone. The latter one operates in a different frequency for each antenna element and is used to obtain the optimum phase that needs to be set for each element to generate a beam in the desired direction, at the main tone frequency. The novel method was applied to linear, planar, 3-D antennas, and noncollocated multiantennas to validate its applicability to different antenna types. Line-of-Sight (LOS) and non-LOS experimental results demonstrate that the method can be used to retrieve the required phase to fully control the antenna radiation pattern. An optimum radiation pattern and lowest error vector magnitude (EVM) can be achieved even under high multipath effects/non-LOS conditions. A comparison between the performance and the application of the array factor (AF) theory is presented for practical indoor scenarios, demonstrating the effectiveness of the method. It is demonstrated that the method may be an alternative to the calibration of nonstandard MIMO antennas, where the AF computation is complex or not possible.**

***Index Terms*— Beamforming, calibration, multiple-input multiple-output (MIMO) antennas, multisine, over-the-air (OTA).**

I. Introduction

MULTIPLE-INPUT multiple-output (MIMO) antennas will achieve large array sizes in the upcoming fifth generation (5G) to achieve directional transmission with a higher gain. Since the individual radiating elements in MIMO antennas are close to each other, the total far-field radiation pattern results from the constructive interference of the individual antenna element pattern, creating the beam. The main purpose of using beamforming is to transmit the signal directly to the target, with a very narrow beam in order to achieve highly efficient transmission, instead of spreading the signal to an entire area. By controlling the phase shift among antenna elements, the desired beam position can be accomplished, and to achieve a higher directivity, the number of elements of antenna array should increase, accordingly. In order to control the antenna array beam direction, the signal radiated from each antenna element should be properly adjusted in phase (and amplitude), based on the antenna array factor (AF) theory, which is based on the superposition of individual patterns of each element, to create the far-field pattern of the array [1]. AF is a function of the positions of the antenna elements in the array and the amplitude/phase used on each. By controlling those parameters, several desired radiation pattern properties can be achieved. Using AF theory, the main beam signal can be steered by controlling the phase of each antenna element, so the maximum radiation direction can be controlled accordingly to the target direction.

There are different types of antenna arrays, such as linear, planar, and conformal (or 3-D). Particularly, in 3-D antenna arrays, the calibration of the radiation pattern can be challenging to obtain with AF theory. Thus, methods that can be used for appropriate calibration are highly desirable to enhance the overall antenna array performance regardless of the deployment scenarios. To this extent, appropriate gain and phase calibrations are requisites for each channel of the MIMO system to ensure optimal system operation [2].

Since accurate amplitude and phase are requirements to accomplish the best performance for this type of antennas, a calibration procedure must be applied; otherwise, several problems in the performance of the antenna array may occur when beamforming is applied. If there are errors in amplitude, the side lobes of the antenna array increase, and the gain will decrease. Also, since power amplifiers (PAs) are usually placed in each RF path, they will contribute with nonideal effects, giving rise to amplitude and phase errors [3]. With respect to phase errors, these have a huge impact on antenna performance, particularly in the main beam direction, unless the phase error is the same across elements although nulls

Manuscript received June 23, 2020; revised September 21, 2020; accepted October 9, 2020. Date of publication November 4, 2020; date of current version January 5, 2021. This work was supported by the European Regional Development Fund (FEDER), through the Regional Operational Programme of Lisbon (POR LISBOA 2020) and the Competitiveness and Internationalization Operational Programme (COMPETE 2020) of the Portugal 2020 framework [Project INFANTE with Nr. 024534 (POCI-01-0247-FEDER-024534)]. The work of Marina Jordão was supported by the Fundação para a Ciência e Tecnologia (F.C.T.) under Ph.D. Grant SFRH/BD/143204/2019. The work of Daniel Belo was supported by F.C.T. under Ph.D. Grant SFRH/BD/142403/2018. This work was sponsored in part by the Roger Pollard Student Fellowship from the Automatic RF Techniques Group. *(Corresponding author: Marina Jordão.)*

Marina Jordão, Daniel Belo, Arnaldo S. R. Oliveira, and Nuno Borges de Carvalho are with the Departamento de Eletrónica, Telecomunicações e Informática, Instituto de Telecomunicações, Universidade de Aveiro, Campus Universitário de Santiago, 3810-193 Aveiro, Portugal (e-mail: marinajordao@ua.pt; a35842@ua.pt; arnaldo.oliveira@ua.pt; nbcarvalho@ua.pt).

Rafael F. S. Caldeirinha is with the Instituto de Telecomunicações, Polytechnic Institute of Leiria, 2411-901 Leiria, Portugal (e-mail: rafael.caldeirinha@ipleiria.pt).

Color versions of one or more of the figures in this article are available online at https://ieeexplore.ieee.org.

Digital Object Identifier 10.1109/TMTT.2020.3032900

are affected by these errors and their duty is to obstruct the interference. For this reason, phase errors between antenna array elements should be kept as low as possible. With this in mind, the calibration of antenna arrays should compensate for nonideal effects, amplitude, and phase mismatch between elements, hardware, and cables [4]. Moreover, in a wireless communication system, where a transmitting (TX) antenna communicates with a receiving (RX) antenna, several effects lead to signal degradation, such as attenuation as a result of absorption and/or fading due to multipath effects, among others. Consequently, the compensation of those effects is important to achieve a successful and efficient communication link, where calibration plays an important role.

In addition, antenna arrays elements both radiate and absorb, and consequently, mutual coupling occurs. The electromagnetic interactions when beamforming is performed will impact on the MIMO system performance. Several solutions can be applied to minimize the impact of mutual coupling in MIMO systems. For instance, by increasing the distance between antenna elements, the mutual coupling can be minimized. However, this methodology will originate antennas with larger dimensions. Thus, in the literature, several works present strategies to avoid mutual coupling [5]–[11].

Over-the-air (OTA) methods are currently being explored to calibrate MIMO antennas in terms of amplitude and phase [1]. Nafe *et al.* [2] describe a method based on mutual coupling. In that work, coupling symmetries were used to calibrate quad antenna arrays through their two neighboring arrays. This means that, to apply the method, the antenna array must be symmetrical and cannot be applied to antennas with an odd number of elements. In other works, such as [12], the authors reuse bidirectional pilot signals that already exist in today's communication systems for calibration. Nevertheless, to apply such methods, the calibration procedure is performed prior to the antenna installation, which does not take into consideration the propagation channel. Hence, an *in situ* phase array calibration is presented in [1], aiming to perform calibration during the communication process by performing channel estimation and it could be performed in real time. However, this method requires higher software processing to apply the estimation methods. The method assumes that phase shifters have a common magnitude, which can lead to phase errors in the estimation procedure. An OTA phased array calibration method based on measured complex array signals with one single probe is presented in [13]. In this method, all array elements are excited simultaneously in the measurement, and the reverse phase of each element is obtained. For this, $N+1$ measurements are required to calibrate the antenna array, where N is the number of the antenna elements. The greater the number of elements of the antenna, the greater the number of measurements required to apply the method, which makes it complex and more time-consuming. In [14], a compact midfield millimeter-wave OTA RF measurement method demonstrates that the antenna array can be calibrated for the far-field environment using midfield measurements. However, the mild-field to far-field correction does not obtain precise measurement results in terms of depth of nulls in antenna patterns because the distance is limited. Thus, when individual antenna patterns are not uniform among elements, the midfield-to-far-field correction error will increase; this means that the method cannot be applied in different types of MIMO antennas. Therefore, calibration can be applied by using diversified approaches for OTA environments or other scenarios. To avoid the problems that arise from the methods described before, additional strategies should be explored. For instance, multisines may be used for different solutions, such as calibration [15]. In [16] and [17], multisines are used to identify MIMO antenna elements during their operation in order to detect possible antenna malfunctions. Multisines have been used in different scenarios, for instance, to perform signal calibration [18]. In [19], a strategy to characterize antenna arrays using tickle tones was demonstrated as a starting point for their characterization. The works developed in [19] and [20] demonstrate new strategies to characterize antenna arrays. The authors show that a multisine consisting of the main tone (equal in all elements) and a tickle tone, with smaller power in relation to the main tone and at different frequencies for each element, may allow us to identify problems within the antenna array.

In this work, the multisines are further explored for another purpose to acquire phase information in order to perform OTA MIMO antenna transmission beam calibration. With this in mind, the main goal of this article is to present an OTA calibration method that controls the MIMO antenna beam in order to generate the best radiation pattern to communicate with a given target, being proposed as an alternative to AF, to perform beamforming. This approach takes advantage of the information provided by a multisine signal, which is then used to compensate for, in real time, the effects of the propagation channel, and the MIMO system itself. In addition, the proposed method is applied to a 3-D MIMO antenna and two noncollocated multiantennas to demonstrate that in MIMO antennas that have different shapes and with an odd number of elements, the application of the method can be an advantage to enable efficient beamforming. This solution to calibrate the OTA MIMO system was designed for MIMO antennas, where there is the freedom to set the desired signal and phase for each antenna element in the digital domain. Consequently, it can be applied to any antenna array configuration if there is the freedom to configure each element independently. Moreover, the method compensates for any mutual coupling and unwanted channel effects, such as multipath. In this OTA multisine system, the method operates based on feedback. From an application point of view, the method may be used for OTA calibration and integrated within a communication protocol for different applications and scenarios. For instance, the communication protocol can include the tickle tones frequency information and their phases. In a multibeam environment, the proposed method can select several frequencies for the tickle tones, which are different from user to user and based on the communication protocol information.

This article is divided as follows. The multisine methodology is explained in detail in Section II. In Section III, the OTA multisine system is described. In addition, the used MIMO antennas and the elaborated algorithm are presented. The line-of-sight (LOS) and non-LOS experimental results

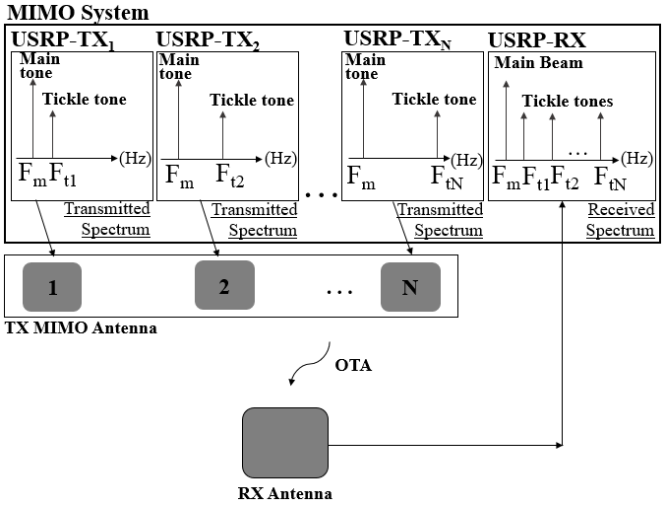

Fig. 1. Representation of the spectrum transmitted by each MIMO antenna element and the spectrum received by the RX antenna in the receiver.

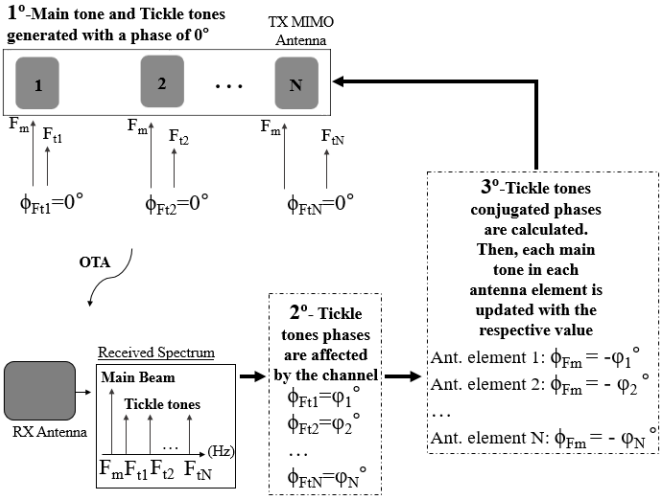

Fig. 2. Theoretical procedure to apply the multisine method.

are presented in Section IV and compared with the ones that result from applying the AF theory directly for different indoor scenarios. Finally, in Section IV, conclusions will be drawn.

II. Multisine Methodology

The concept of using a multisine, main tone (F_m), and tickle tone (F_{ti}) was proposed in [19] and [20] to identify possible malfunctions within an MIMO antenna. However, in contrast to this, in this work, this concept is used to compensate and calibrate the antenna main beam (at F_m) by obtaining the phase information of each MIMO antenna element from its respective tickle tone (F_{ti}). The multisine consists of the main tone (F_m), fed equally to all antenna elements and used as the MIMO beamforming carrier, and an additional tickle tone (F_{ti}). Each antenna element is associated with different tickle tones that operate at different frequencies. The main tone operates at the same frequency and amplitude in all MIMO antenna elements. On the contrary, the tickle tone operates in different frequencies in each MIMO antenna element, presenting a small amplitude compared with the main tone.

A. Procedure Description

As an example, Fig. 1 demonstrates the multisine method used in this work, for an MIMO antenna composed of N elements. A transmitter (TX) is connected to each MIMO antenna element that generates the main tone (F_m) and the tickle tone (F_{ti}). Each MIMO antenna element is then fed with two tones. The signal propagates to the receiver (RX), which is connected to the RX antenna, and obtains the main tone and the tickle tones contribution of each antenna element. In summary, in the RX antenna, the main tone and all the tickle tones are acquired, as represented in Fig. 1. Then, the tickle tones' phases are obtained, providing information about the perturbations from each propagation path. Subsequently, that information is used to synthesize a radiation pattern that improves the TX MIMO antenna operation.

To perform beamforming in MIMO antennas, the specific phase distribution is required across the individual antenna element and should be given by the AF [21]. However, when signals are transmitted to the target, each of them is affected by its channel response, which can undesirably decrease their overall performance if they are highly uncorrelated. Using the tickle tones' phase values that were received by the RX antenna and by applying the conjugate of those values to the main tone of each corresponding TX antenna element, the antenna beam will be oriented to the RX antenna. In summary, the main tone phase vector of the transmitters is updated with the conjugate phase of the phases acquired by the receiver. Fig. 2 demonstrates this theoretical procedure. First, the main tone (F_m) and the tickle tones (F_{t1}, F_{t2}, …, F_{tN}) are generated with a phase of 0°. Then, the TX MIMO antenna transmits this data, and the RX antenna acquires the tickle tones information, where each tickle tone presents a different phase value (φ_1, φ_2, …, φ_N). This occurs due to channel effects. In the end, the tickle tones conjugated phases are calculated, and each TX MIMO antenna element's main tone is updated with the respective value ($-\varphi_1$, $-\varphi_2$, …, $-\varphi_N$). By applying this strategy, the tickle tones provide information to establish an improved communication link between TX and RX while taking into consideration the propagation channel.

III. OTA Multisine System

In order to validate the proposed method, the OTA block diagram depicted in Fig. 1 was implemented in a laboratory environment, as shown in Fig. 3. The setup consists of three main components: a TX MIMO antenna, to perform beamforming (in this work, three types of MIMO antennas are used, which will be described in the following), an RX antenna, and an MIMO system to control the experimental setup consisting of several transmitters and receivers. The MIMO system is composed of eight software-defined radios (SDRs), universal software radio peripheral (USRP), 16 transmitters, and 16 receivers. However, in this work, only one receiver is used, where the others remain disabled. Those transmitters are

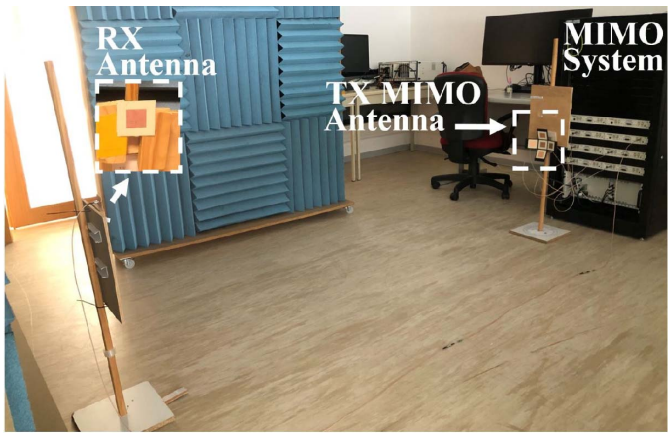

Fig. 3. Laboratorial measurement setup.

Fig. 4. Linear MIMO antenna.

connected to the MIMO antenna elements. The RX antenna is connected to one receiver. All TX MIMO antenna elements are fed synchronously and simultaneously. Each transmitter generates its multisine (main tone and its respective tickle tone) to the TX MIMO antenna element. The RX antenna is positioned in the far-field region and connected to the USRP that is in the receiving mode and used to sample the information received by the RX antenna. Hence, from the RX antenna tickle tones' phases, each phase of the main tone is updated with the conjugate value of the corresponding received tickle tone. By doing so, a beam that is properly aligned with the RX antenna is obtained.

A. MIMO Antennas

The proposed multisine OTA method was tested with five different types of MIMO transmitting antennas: a linear, a planar, a 3-D array, and two noncollocated multiantennas. The linear MIMO antenna consists of seven elements operating at 2.587 GHz, as shown in Fig. 4. The planar antenna operates at the same frequency and consists of six elements, two rows, and three columns, as illustrated in Fig. 5. These two conventional antennas have an interelement spacing of $\lambda_0/2$ (λ_0 is the free-space wavelength). The 3-D antenna consists of five elements, with an interelement spacing of $0.4691\lambda_0$ and operating at 2.6 GHz. The 3-D antenna elements are positioned on a concave surface, with elements 2, 3, 4, and 5 with a tilt of 25° with respect to the center element (element 1), as illustrated in Fig. 6. The RX antenna is a single patch tuned to 2.6 GHz, with a bandwidth of 30 MHz, as shown in Fig. 3.

Furthermore, a noncollocated multiantenna system operating at 5.6 GHz was used, which is illustrated in Fig. 7. This multiantenna consists of seven identical antennas placed uneven, so as to represent a random deployment, as depicted

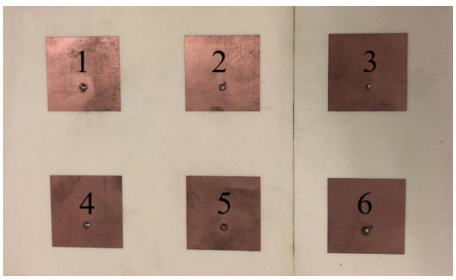

Fig. 5. Planar MIMO antenna.

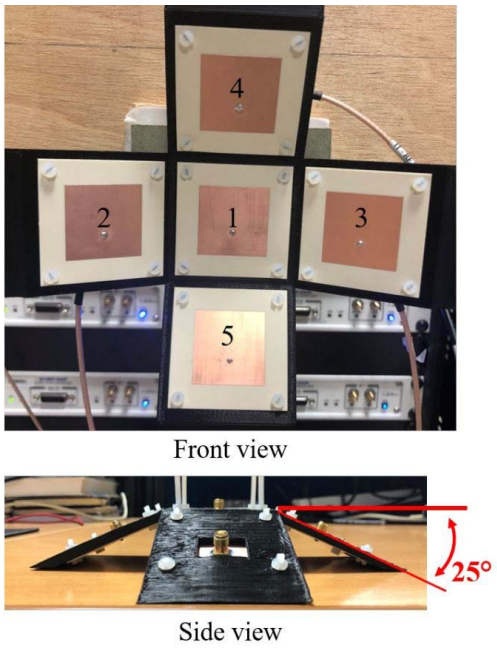

Fig. 6. 3-D MIMO antenna.

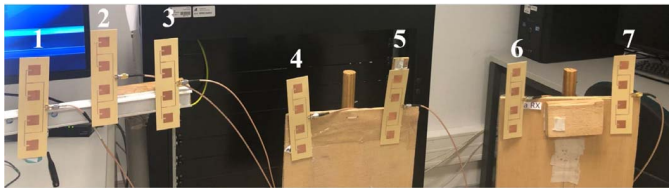

Fig. 7. Noncollocated multiantenna with equal elements.

in Fig. 7. Another noncollocated multiantenna system operating at 5.6 GHz and composed of seven antenna elements was used, and the antenna elements were uneven, but, in this case, the seven elements are not equal. With this in mind, four elements of the previous noncollocated multiantennas and three patch elements form this noncollocated multiantenna with different elements were used. The patch antennas were also built with Isola IS680 (h = 30 mil and Dk=3.38) substrate. Fig. 8 depicts noncollocated multiantenna with different elements. In addition to these two noncollocated multiantennas operating at 5.6 GHz, a single patch antenna tuned to the same frequency was used in the receiver. All antennas were built with Isola IS680 (h = 30 mil and Dk = 3.38) substrate.

Fig. 8. Noncollocated multiantenna with different elements.

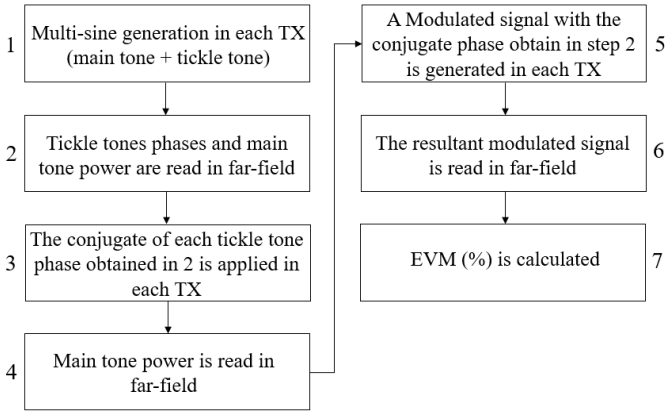

Fig. 9. Algorithm description.

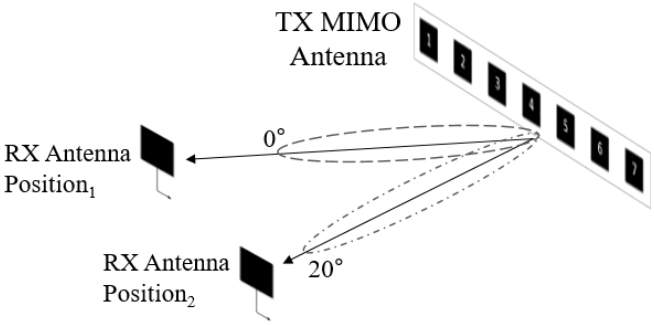

Fig. 10. Measurement geometry considering the RX antenna at two different positions.

B. Algorithm

To control the whole setup using the proposed calibration OTA multisine, a specific algorithm was developed. The algorithm is represented by a flowchart, as shown in Fig. 9. The first step of the algorithm is to generate the main tone and the tickle tone for each transmitter antenna element. In this step, the frequencies of the main tone and the tickle tones are selected, as well as the amplitude. If the user requires a higher or smaller power in tickle tones and main tone, to obtain a higher or a smaller received signal in the RX antenna, the power values can be selected. Moreover, the user can select at which frequency can generate each tickle tones closer or distant from the main tone. In the second step of

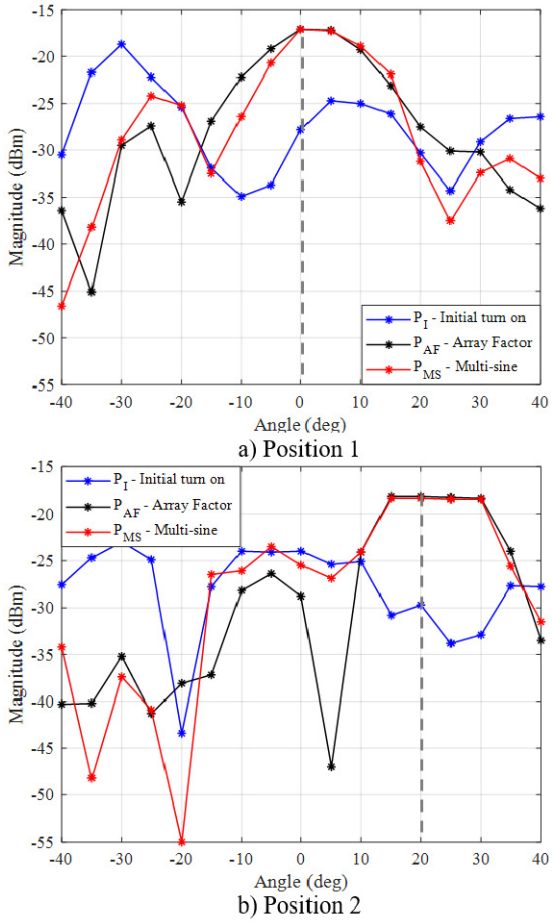

Fig. 11. Linear MIMO antenna radiation pattern for P_I, P_{AF}, and P_{MS} in (a) position 1 and (b) position 2. The dashed line represents the receiver direction.

the algorithm, in far-field, the main tone signal amplitude and tickle tones phases are obtained by the RX antenna, through the receiver, and their conjugate is calculated. In other words, from the phase information of each tickle tone obtained in the RX antenna, the respective main tone magnitude in each antenna element remains equal, but the phase is updated with their conjugate. For example, if the tickle tone 1 presented in the RX antenna yields a phase value of 10°, the conjugate value calculated in step 2 is −10°, consequently, the respective main tone for this tickle tone is updated with a new phase value. In the third step, the conjugated phases are applied to the main tone for each TX. This means that the main tone is aligned to the receiver. After these steps, in the fourth step, the power collected by the RX antenna from the main tone is measured to compare the main tone power before and after applying the method and this way to draw the far-field radiation pattern. Afterward, in the transmitters, the multisine (main tone and tickle tone) is replaced by an M-QAM modulated signal. In the fifth step, this modulated signal is transmitted in each transmitter with the conjugate phase obtained in step 2. This means that the modulated signal excites each TX antenna element with the respective phase value (calculated in step 2) in order to achieve the main signal calibrated to the receiver. In the far-field, the radiation pattern is obtained in the sixth step, and in the final step,

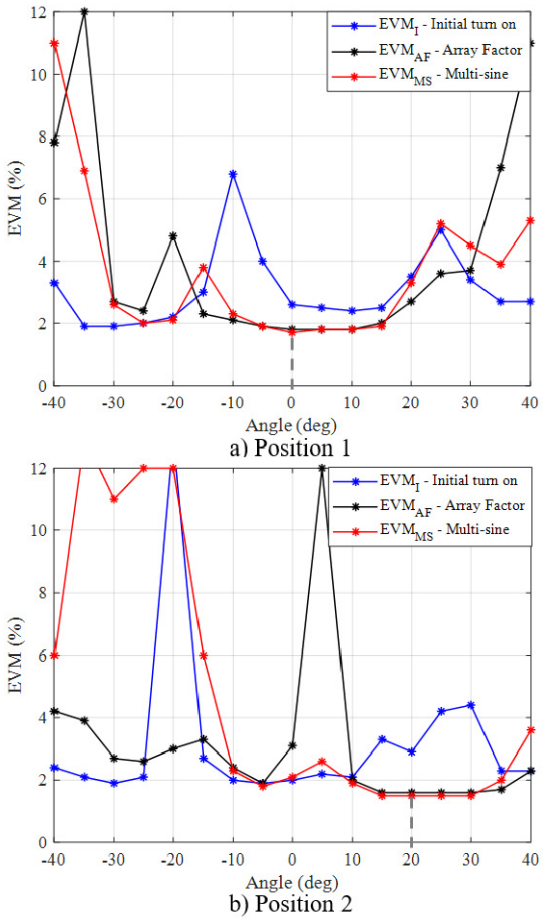

Fig. 12. Linear MIMO antenna EVM for P_I, P_{AF}, and P_{MS} in (a) position 1 and (b) position 2. The dashed line represents the receiver direction.

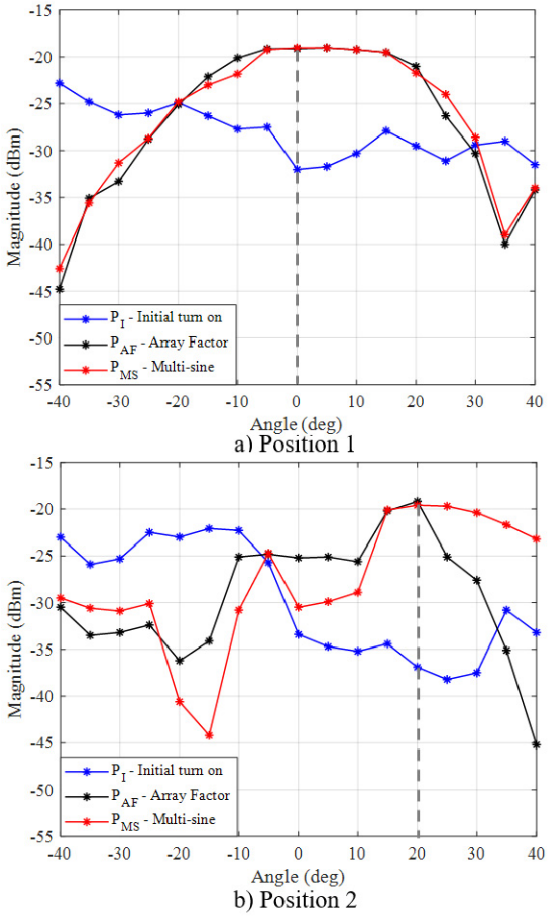

Fig. 13. Planar MIMO antenna radiation pattern for P_I, P_{AF}, and P_{MS} in (a) position 1 and (b) position 2. The dashed line represents the receiver direction.

the error vector magnitude (EVM) is calculated in order to have a figure of merit to validate the link communication.

IV. Measurements

Several experiments were performed in order to validate the proposed OTA multisine calibration. Fig. 10 illustrates the experimental setup, showing the location of the RX antenna for each experiment. In the first position, position 1, the RX antenna is placed on the broadside direction of the TX MIMO antenna. For the second position, position 2, the RX antenna was placed 20° off of the broadside direction. For each of those two positions, measurements were performed for the linear, planar, and 3-D antennas.

A. Line-of-Sight Measurement

When the MIMO system is turned on, the transmitters awake synchronized with random initial phases. Thus, to perform beamforming, by using the AF [22], for the linear and planar MIMO antennas, the first step of the calibration method described in [21] was followed. This step was carried out to provide a reference point for comparison purposes between the OTA multisine method and the direct application of the AF theory. With the OTA multisine method, the frequencies

TABLE I

Baseband Multisine Frequencies Used in Each Port of the Five MIMO Transmitting Antennas

	F_m (Hz)	F_{t1} (Hz)	F_{t2} (Hz)	F_{t3} (Hz)	F_{t4} (Hz)	F_{t5} (Hz)	F_{t6} (Hz)	F_{t7} (Hz)
Linear (7 ports)	10k	4k	6k	8k	12k	14k	16k	18k
Planar (6 ports)	10k	4k	6k	8k	12k	14k	16k	-
3D (5 ports)	10k	4k	6k	8k	12k	14k	-	-
Non-collocated multi-antenna with equal elements (7 ports)	10k	4k	6k	8k	12k	14k	16k	18k
Non-collocated multi-antenna with different elements (7 ports)	10k	4k	6k	8k	12k	14k	16k	18k

of the multisine that were selected for each port of the MIMO transmitting antennas are shown in Table I. The selection of tickle tones frequencies aiming to avoid intermodulation with the main tone. In terms of power, the main tone (F_m) and the tickle tones (F_{ti}) have a difference of 10 dB. It is not required high power levels for the tickle tones, just enough to obtain its

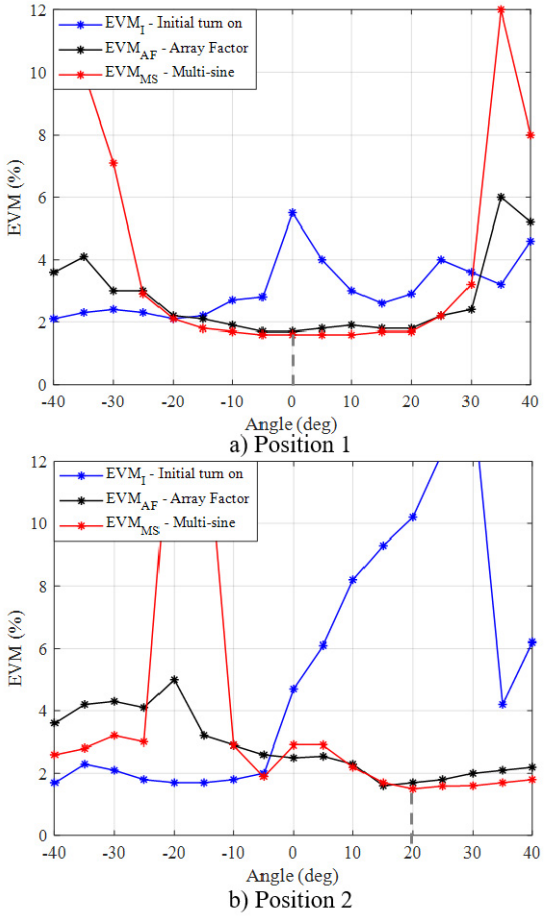

Fig. 14. Planar MIMO antenna EVM for P_I, P_{AF}, and P_{MS} in (a) position 1 and (b) position 2. The dashed line represents the receiver direction.

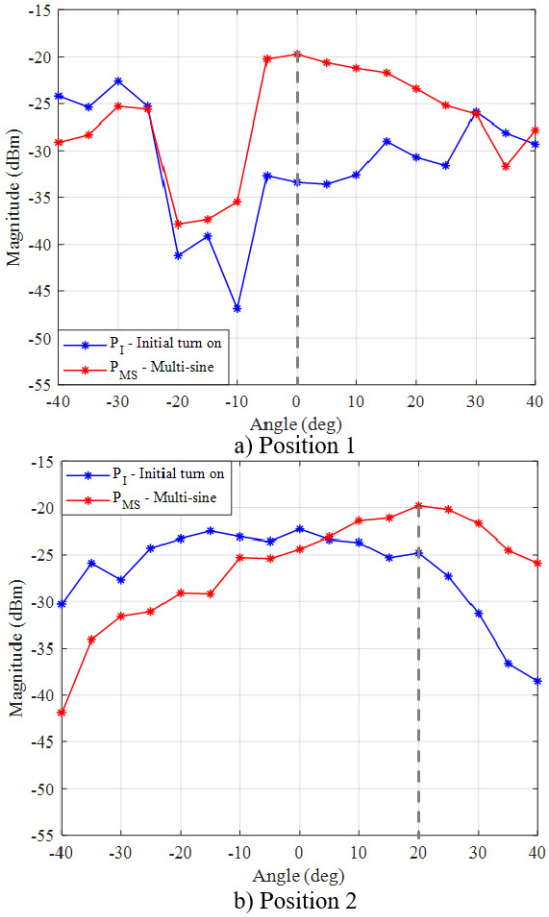

Fig. 15. 3-D MIMO antenna radiation pattern for P_I and P_{MS} in (a) position 1 and (b) position 2. The dashed line represents the receiver direction.

information in the receiving antenna. This means that, to use the method, the tickle tone's power levels do not require the same power as the main tone.

Thus, following the algorithm presented in Section III, the radiation pattern of the MIMO transmitting antennas was obtained. The results for the linear MIMO transmitting antenna are presented in Fig. 11, for both positions. P_I is the initial power received by the RX antenna when the system is turned on (with random initial phases). $P_{AF}$is the power received by the RX antenna when the AF theory is directly applied, and P_{MS} is the final received power from the application of the optimum phase distribution among transmitting elements provided by the proposed multisine method. This method can be an alternative to perform MIMO antenna beamforming. It should be noted that all the measurements were performed within a strong multipath environment (inside a laboratory with several objects around), leading to fluctuations in the received power (P_{AF}). Moreover, after using the OTA multisine method to calibrate the MIMO antenna beam, a 64-QAM modulated signal was used to evaluate the operation of the method with conventional modulated signals, and the EVM (%) was calculated. The EVM achieved for the linear MIMO transmitting antenna in positions 1 and 2 is shown in Fig. 12. For the planar MIMO transmitting antenna in positions 1 and 2, the achieved radiation patterns are shown in Fig. 13 and the

TABLE II

LOS RESULTS FOR LINEAR AND PLANAR MIMO ANTENNAS, COMPARING THE AF METHOD WITH OTA MULTISINE METHOD

	Linear		Planar	
Position	**Position 1 0°**	**Position 2 20°**	**Position 1 0°**	**Position 2 20°**
P_{AF} (dBm)	-17.1	-18.1	-19.1	-19.2
P_{MS} (dBm)	-17.1	-18.3	-19	-19.6
EVM_{AF}(%)	1.8	1.6	1.7	1.7
EVM_{MS}(%)	1.7	1.5	1.6	1.5

EVM in Fig. 14. Those results are summarized in Table II for positions 1 and 2. By analyzing Figs. 11 and 13 and Table II, it can be concluded that the multisine method is comparable to the AF since the results are very similar for the position directions where the beam must be pointed. The same statement is valid for the EVM results since the obtained EVM is closer, presenting the OTA multisine method best results than the AF. This occurs because the OTA multisine method compensates for the multipath effects, leading to an increase in the received signal strength at the RX antenna.

Besides linear and planar MIMO antennas, there are other types of transmitting antennas. For instance, 3-D MIMO antennas are being used in different scenarios, for example,

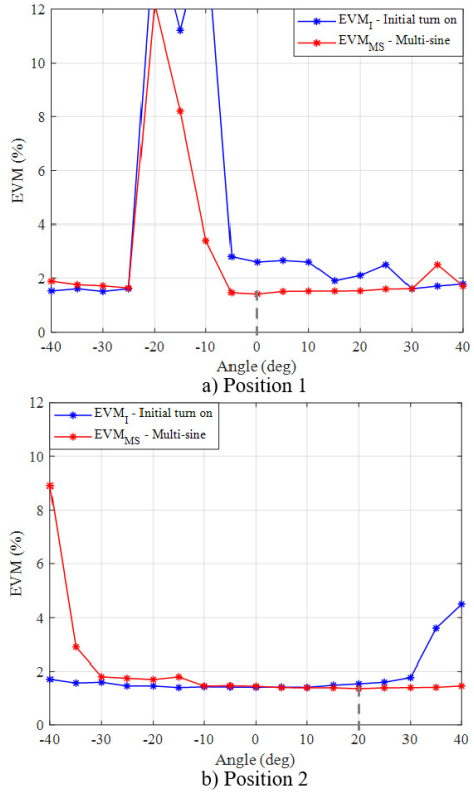

Fig. 16. 3-D MIMO antenna EVM for P_I and P_{MS} in (a) position 1 and (b) position 2. The dashed line represents the receiver direction.

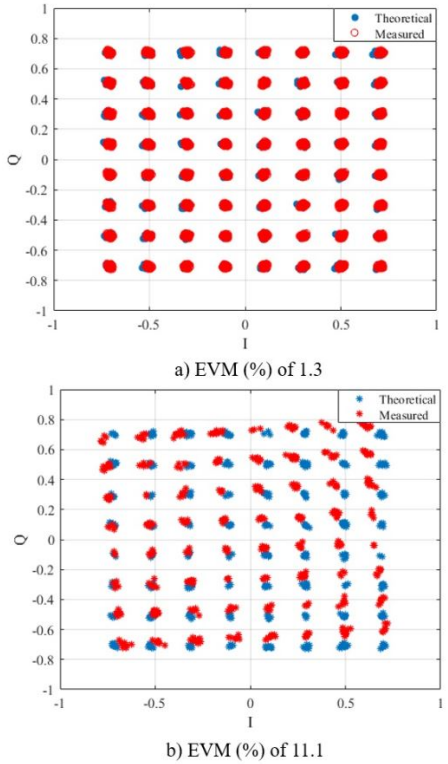

Fig. 17. High and lower 3-D MIMO antenna EVM results.

in maritime [23] and satellite communications [24]. With this type of MIMO antennas, additional challenges arise, being one of them the exact AF calculation to perform beamforming.

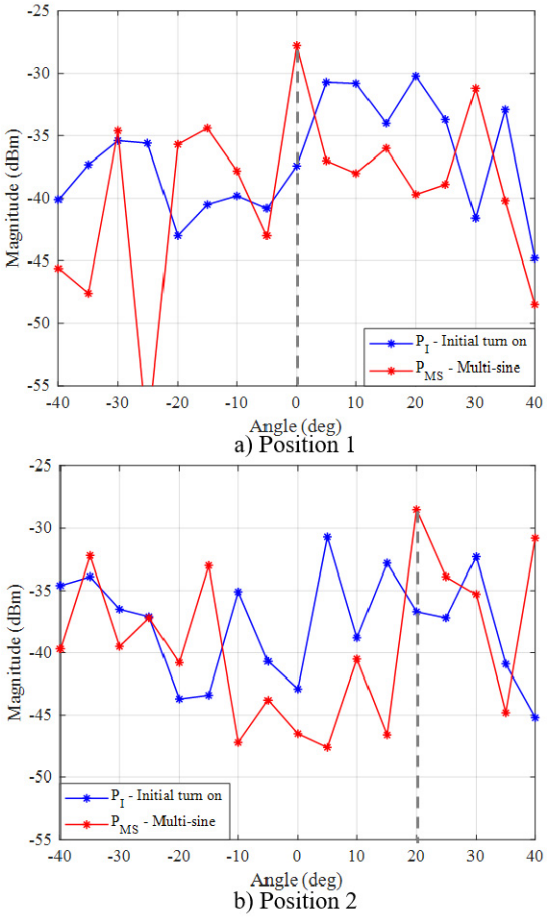

Fig. 18. Noncollocated multiantenna with equal elements' radiation pattern for P_I and P_{MS} in (a) position 1 and (b) position 2. The dashed line represents the receiver direction.

The 3-D MIMO antenna described in Section III was used to demonstrate the relevance of the method for those situations. In this particular case, the antenna elements are placed on a concave surface, with the outer elements with a tilt of 25° with respect to the center element. For that matter, the OTA multisine method was performed with the 3-D antenna; however, its performance was not compared with the AF because it is not known or difficult to obtain the mathematical formulation to apply the AF on this type of antenna. The radiation pattern results are presented in Fig. 15 for positions 1 and 2. As it can be seen, the 3-D MIMO antenna beam is properly aligned with the receiving antenna, for both positions. In Fig. 16, the EVM results for the 3-D antenna are also shown, demonstrating that the highest EVM was obtained for both desired positions, position 1 and position 2, as expected. Moreover, Fig. 17 shows the highest and the lowest EVM values obtained for position 1.

With the same goal of using the 3-D antenna to demonstrate the importance of the method for the cases where calibration of the antenna beam is a challenge, for instance, nonstandard MIMO antennas, a noncollocated multiantenna with equal elements was selected. As mentioned previously, this antenna is composed of seven equal elements distributed irregularly, as depicted in Fig. 7, and, consequently, its beamforming coefficients are unknown. With this in mind, the method

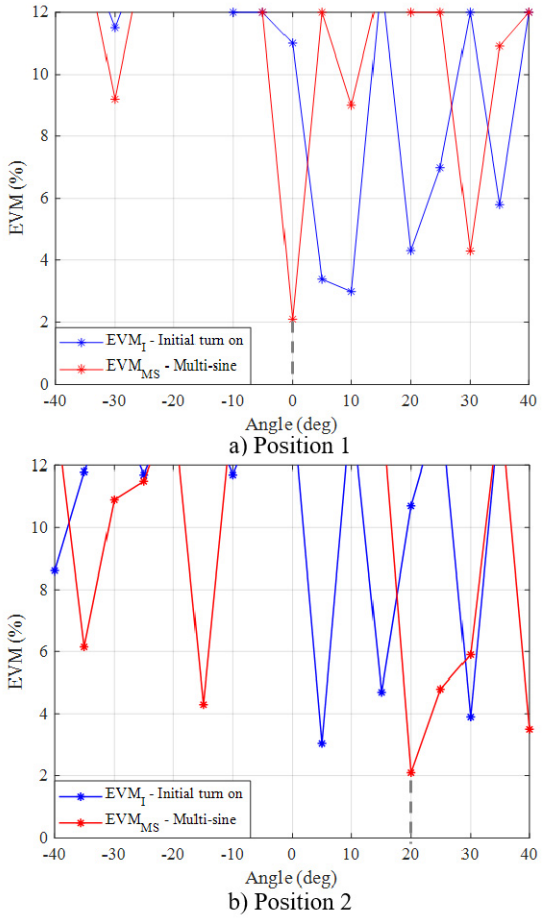

Fig. 19. Noncollocated multiantenna with equal elements' EVM for P_I and P_{MS} in (a) position 1 and (b) position 2. The dashed line represents the receiver direction.

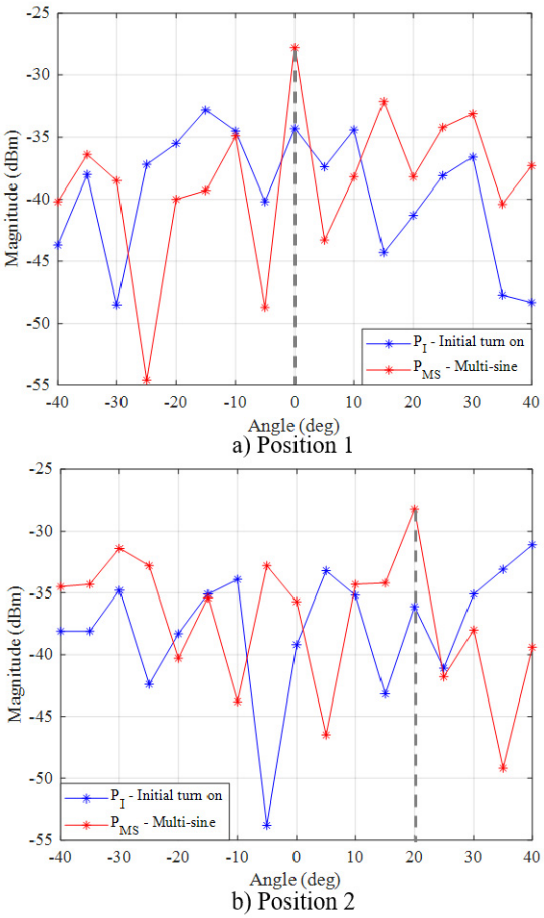

Fig. 20. Noncollocated multiantenna with different elements' radiation patterns for P_I and P_{MS} in (a) position 1 and (b) position 2. The dashed line represents the receiver direction.

was applied to this antenna for positions 1 and 2, and the radiation pattern results were obtained, as presented in Fig. 18. It becomes clear from these results that the beam alignment technique is effective for both positions 1 and 2. This is further complemented by the EVM results obtained for both positions, as presented in Fig. 19, clearly demonstrating the technique's effectiveness. The second experiment was performed with the same noncollocated multiantenna but with different elements, as illustrated in Fig. 8. Since this antenna is composed of two different types of antennas elements, as described in Section III, the challenge to obtain the beam calibration arises. Therefore, the proposed calibration method was applied to this antenna for positions 1 and 2, respectively. As expect and demonstrated by the radiation pattern results in Fig. 20, the beam was aligned accordingly for positions 1 and 2, respectively. The EVM results for this antenna are depicted in Fig. 21, in which the lowest EVM values were obtained for both positions.

B. Non-Line-of-Sight Measurement

A non-LOS experiment was performed to demonstrate that by using the multisines phase information, the MIMO antenna beam can be properly adjusted to align with the target, and it can be an advantage compared with AF, for example, in a real scenario when an object is between the TX and the RX. To this extent, a metal plane was introduced between the MIMO transmitting antenna and the receiving antenna, as presented in Fig. 22. This experiment was performed for both antennas, linear, and planar MIMO antennas, in positions 1 and 2. The results are shown in Table III, demonstrating that the OTA multisine method achieves higher performance than the AF theory, especially when modulated signals are transmitted. In the linear MIMO transmitting antenna case, the OTA multisine method presents higher performance than AF because the power received by the RX antenna is 1.6 dB higher than the one that is possible to receive with the

TABLE III
NON-LIGHT-OF-SIGHT FOR LINEAR AND PLANAR MIMO ANTENNAS, COMPARING THE AF METHOD WITH OTA MULTISINE METHOD

	Linear		Planar	
Position	**Position 1 0°**	**Position 2 20°**	**Position 1 0°**	**Position 2 20°**
P_{AF} (dBm)	-31.6	-26.3	-32.9	-29.4
P_{MS} (dBm)	-30	-26.5	-32.7	-29.4
EVM_{AF} (%)	4.6	2.4	5.3	2.8
EVM_{MS}(%)	4.1	2.3	3.9	2.7

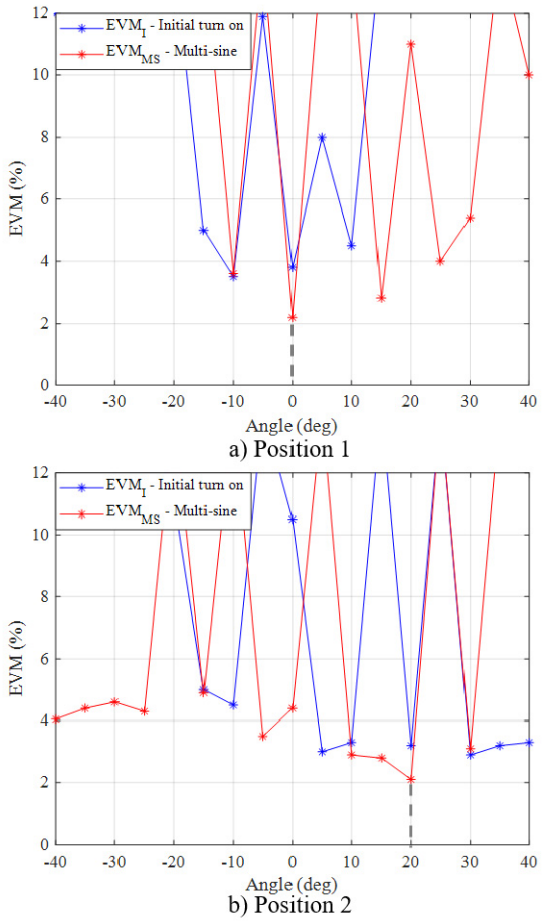

Fig. 21. Noncollocated multiantenna with different elements' EVMs for P_I and P_{MS} in (a) position 1 and (b) position 2. The dashed line represents the receiver direction.

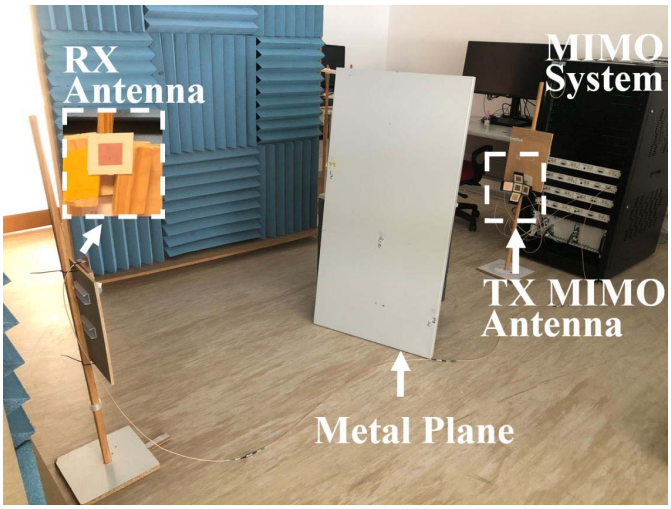

Fig. 22. Non-LOS experiment, where a metal plane with a considerable size was introduced to cover the direct transmission of the signal between the TX and the RX antennas.

application of the AF. In addition, with the proposed method, the EVM shows an improvement of 0.5% compared with AF. Furthermore, with the planar antenna, it is evident that, in position 2, the AF method presents a higher EVM than the one achieved by the proposed method.

TABLE IV

NON-LIGHT-OF-SIGHT EXPERIMENT RESULTS FOR 3-D MIMO ANTENNA, NONCOLLOCATED MULTIANTENNA WITH EQUAL ELEMENTS, AND NONCOLLOCATED MULTIANTENNA WITH DIFFERENT ELEMENTS

	3D		Non-collocated with equal elements		Non-collocated with different elements	
Position	**Position 1 0°**	**Position 2 20°**	**Position 1 0°**	**Position 2 20°**	**Position 1 0°**	**Position 2 20°**
P_{MS} (dBm)	-32.1	-33.2	-38.7	-39.3	-36	-34
EVM_{MS} (%)	5.1	6.2	9.7	11.1	9.8	5.6

TABLE V

COMPARISON BETWEEN OTA CALIBRATION METHODS PRESENTED IN LITERATURE WITH THE PROPOSED METHOD, I.E., OTA MULTISINE CALIBRATION METHOD

	Characteristics of the methods	**OTA multi-sine calibration method characteristics**
Method [1]	Based on channel estimation methods, which require higher software processing; It is assumed that phase shifters have a common magnitude, which can lead to phase errors in the estimation procedure.	It is a real-time calibration; No estimation is considered; Lower software processing.
Method [2]	Only for symmetrical antenna arrays; Only for antenna arrays with even number of elements.	For any type of standard and non-standard antenna arrays; For antenna arrays with even and odd elements.
Method [12]	Calibration is applied prior to antenna commission; Propagation channel is not considered.	It is a real-time calibration; Propagation channel is considered.
Method [13]	When the number of antenna elements increase the method increase the complexity; Higher time-consuming.	The number of antenna elements does not interfere with the complexity of the method, so less software complexity; Less time-consuming.
Method [14]	Cannot be applied in different type of MIMO antennas, because when individual antenna patterns are not uniform among elements, the midfield-to-far-field correction error will increase.	For any type of standard and non-standard antenna arrays; For antenna arrays with even and odd elements.

Also, for the 3-D MIMO antenna, consisting of noncollocated multiantenna with equal elements and noncollocated multiantenna with different elements, a non-LOS experiment was performed. Results presented in Table IV clearly demonstrate that when a metal plane is placed in the radio path between the TX and RX antennas, the calibration method achieves the goal of a properly adjusted beam aligned with the target. However, for these antennas, the AF cannot be applied, and consequently, a comparison cannot be performed.

V. CONCLUSION

In this work, an OTA MIMO antenna calibration using a multisine approach is proposed. The information provided

by a multisine is used to calibrate an MIMO transmitting antenna to align its main beam with a receiving antenna. LOS experimental results demonstrated that, for three different types of MIMO transmitting antennas (linear, planar, and 3-D), by using the OTA multisine method, the beam can be aligned with the target. With this approach, multipath effects, mutual coupling, and system impairments are compensated simultaneously. Moreover, non-LOS experimental results indicate that the OTA multisine method presents better performance than AF. Compared with AF theory, the OTA multisine method presents a faster and simple process to calibrate different types of MIMO transmitting antennas. With a simple initial calibration, the proposed method calibrates the beam accordingly to the MIMO antennas and the propagation channel and can be applied in real time. In addition, it is demonstrated that the method can be used for nonstandard shapes. For the 3-D MIMO antenna with an odd number of elements and noncollocated multiantennas with equal and with different elements, which can be used in distributed systems, where the AF is not known or difficult to obtain, it has been demonstrated that the OTA multisine method can effectively contribute to the proper alignment of the TX antenna beam with the target. The method can be used in different application scenarios and applied to a multiuser environment. The information of the phase of each tickle tone can be integrated with a communication protocol, without requiring a dedicated feedback system, for the TX antenna main beam signal remains aligned with the RX antenna (user) when this one is moving. This way, while RX is moving, the method updates the main beam signal to provide calibration during the movement.

Table V presents a comparison between the proposed calibration method, using multisines, with the other OTA calibration methods presented in the literature, where the benefits of the proposed method are highlighted. To test and calibrate antenna arrays in far-field, usually complex setups with mechanical capabilities are required. By using this method, the test and calibration can be greatly simplified. The method is more economic, with less hardware implementation, reduced computational complexity, less time consumption, and not depending on the number of elements of the antenna array.

REFERENCES

[1] T. Moon, J. Gaun, and H. Hassanieh, "Online millimeter wave phased array calibration based on channel estimation," in *Proc. IEEE 37th VLSI Test Symp. (VTS)*, Apr. 2019, pp. 1–6.

[2] A. Nafe, K. Kibaroglu, M. Sayginer, and G. M. Rebeiz, "An *in-situ* self-test and self-calibration technique utilizing antenna mutual coupling for 5G multi-beam TRX phased arrays," in *IEEE MTT-S Int. Microw. Symp. Dig.*, Jun. 2019, pp. 1229–1232.

[3] M. Kottkamp and C. Rowell, "Antenna array testing—Conducted and over the air: The way to 5G," Rohde & Schwarz, Munich, Germany, White Paper 1MA286, Nov. 2016.

[4] K. R. Dandekar, H. Ling, and G. Xu, "Smart antenna array calibration procedure including amplitude and phase mismatch and mutual coupling effects," in *Proc. IEEE Int. Conf. Pers. Wireless Commun. Conf.*, Dec. 2000, pp. 293–297.

[5] H. S. Farahani, M. Veysi, M. Kamyab, and A. Tadjalli, "Mutual coupling reduction in patch antenna arrays using a UC-EBG superstrate," *IEEE Antennas Wireless Propag. Lett.*, vol. 9, pp. 57–59, 2010.

[6] M. Alibakhshikenari *et al.*, "Interaction between closely packed array antenna elements using meta-surface for applications such as MIMO systems and synthetic aperture radars," *Radio Sci.*, vol. 53, no. 11, pp. 1368–1381, Nov. 2018.

[7] A. Yu and X. Zhang, "A novel method to improve the performance of microstrip antenna arrays using a dumbbell EBG structure," *IEEE Antennas Wireless Propag. Lett.*, vol. 2, pp. 170–172, 2003.

[8] M. Alibakhshikenari *et al.*, "Study on isolation improvement between closely-packed patch antenna arrays based on fractal metamaterial electromagnetic bandgap structures," *IET Microw., Antennas Propag.*, vol. 12, no. 14, pp. 2241–2247, Nov. 2018.

[9] J. OuYang, F. Yang, and Z. M. Wang, "Reducing mutual coupling of closely spaced microstrip MIMO antennas for WLAN application," *IEEE Antennas Wireless Propag. Lett.*, vol. 10, pp. 310–313, 2011.

[10] M. T. Islam and M. S. Alam, "Compact EBG structure for alleviating mutual coupling between patch antenna array elements," *Prog. Electromagn. Res.*, vol. 137, pp. 425–438, 2013.

[11] M. Alibakhshikenari *et al.*, "Meta-surface wall suppression of mutual coupling between microstrip patch antenna arrays for THz-band applications," *Prog. Electromagn. Res. Lett.*, vol. 75, pp. 105–111, 2018.

[12] M. Gustafsson, J. Aulin, M. Hogberg, M. Alm, and B. Sihlbom, "Impact of mutual coupling on capacity in large MIMO antenna arrays," in *Proc. 8th Eur. Conf. Antennas Propag. (EuCAP)*, Apr. 2014, pp. 2723–2727.

[13] F. Zhang, W. Fan, Z. Wang, Y. Zhang, and G. F. Pedersen, "Improved over-the-air phased array calibration based on measured complex array signals," *IEEE Antennas Wireless Propag. Lett.*, vol. 18, no. 6, pp. 1174–1178, Jun. 2019.

[14] H. Kong, Z. Wen, Y. Jing, and M. Yau, "Midfield over-the-air test: A new OTA RF performance test method for 5G massive MIMO devices," *IEEE Trans. Microw. Theory Techn.*, vol. 67, no. 7, pp. 2873–2883, Jul. 2019.

[15] F. Rusek, D. Persson, B. Kiong Lau, E. G. Larsson, T. L. Marzetta, and F. Tufvesson, "Scaling up MIMO: Opportunities and challenges with very large arrays," *IEEE Signal Process. Mag.*, vol. 30, no. 1, pp. 40–60, Jan. 2013.

[16] R. Stuhlfauth and C. Rowell, "3D over-the-air testing of 5G massive MIMO antenna arrays," *Microw. J.*, vol. 60, no. 3, pp. 38–46, 2017.

[17] Z. Zheng, K. Liu, W.-Q. Wang, Y. Yang, and J. Yang, "Robust adaptive beamforming against mutual coupling based on mutual coupling coefficients estimation," *IEEE Trans. Veh. Technol.*, vol. 66, no. 10, pp. 9124–9133, Oct. 2017.

[18] W. Van Moer and Y. Rolain, "A multisine based calibration for broadband measurements," in *Proc. IEEE Instrum. Meas. Technol. Conf. IMTC*, May 2007, p. 16.

[19] D. C. Dinis, N. B. Carvalho, A. S. R. Oliveira, and J. Vieira, "Over the air characterization for 5G massive MIMO array transmitters," in *IEEE MTT-S Int. Microw. Symp. Dig.*, Jun. 2017, pp. 1441–1444.

[20] M. Jordão, D. Belo, and N. B. Carvalho, "Active antenna array characterization for massive MIMO 5G scenarios," in *Proc. 91st ARFTG Microw. Meas. Conf. (ARFTG)*, Philadelphia, PA, USA, Jun. 2018, pp. 1–4.

[21] M. Hefnawi, J. Gai, and R. A. Elasoued, "Mutual coupling effects on MIMO-adaptive beamforming systems," in *Proc. Int. Conf. Netw. Services (ICNS)*, Jun. 2007, p. 106.

[22] A. E. Zooghby, *Smart Antenna Engineering*, 1st ed. Norwood, MA, USA: Artech House, 2005.

[23] M. Geissler, M. Bottcher, R. Gieron, M. Eube, and P. Siatchoua, "A low-cost phased array for mobile satellite communications," in *Proc. 2nd Int. ITG Conf. Antennas*, Mar. 2007, pp. 148–152.

[24] M. Geissler *et al.*, "L-band phased array for maritime satcom," in *Proc. IEEE Int. Symp. Phased Array Syst. Technol.*, Oct. 2010, pp. 518–523.

Marina Jordão (Graduate Student Member, IEEE) received the M.Sc. degree in electronics and telecommunications engineering from the University of Aveiro, Aveiro, Portugal, in 2015, where she is currently pursuing the Ph.D. degree.

Since 2016, she has been a Researcher with the Instituto de Telecomunicaes, Aveiro. Her current research interests include RF measurements and characterization, over-the-air (OTA) characterization, software-defined radio (SDR), mixed-signal characterization, and multiple-input multiple-output (MIMO) antenna arrays characterization.

Ms. Jordão was a recipient of the 2020 Silver Award of ARFTG Roger Pollard Student Fellowship in microwave measurements.

Daniel Belo (Member, IEEE) received the M.Sc. degree in electronics and telecommunications engineering from the University of Aveiro, Aveiro, Portugal, in 2014, where he is currently pursuing the Ph.D. degree.

He has been a Researcher with the Instituto de Telecomunicações, Aveiro, since 2013. His current research interests include microwave electronic circuits, wireless power transfer systems, and analog/digital control.

Rafael F. S. Caldeirinha (Senior Member, IEEE) was born in Leiria, Portugal, in 1974. He received the B.Eng. degree (Hons.) in electronic and communication engineering and the Ph.D. degree in radiowave propagation with a focus on vegetation studies at frequencies from 1 to 62.4 GHz from the University of Glamorgan, Pontypridd, U.K., in 1997 and 2001, respectively.

He is currently the Head of the Antennas & Propagation (A&P-Lr) Research Group, Instituto de Telecomunicações, Leiria, and a Coordinator Professor of mobile communications with the School of Technology and Management (ESTG), Polytechnic of Leiria, Leiria. He has authored or coauthored more than 150 articles in conferences and international journals and four contributions to ITU-R Study Group, which formed the basis of the ITU-R P.833-5 (2005) recommendation. His research interests include studies of radiowave propagation through vegetation media including under wildfires environments, radio channel sounding and modeling, and frequency selective surfaces, for applications at microwave and millimeter-wave frequencies.

Dr. Caldeirinha is also a Fellow Member of Institution of Engineering and Technology (IET). He is also a member of the Editorial Board of the *International Journal of Communication Systems* (IJCS) (New York, NY, USA: Wiley). He was the Program Chair of the WINSYS International Conference from 2006 to 2012 and an Appointed Officer for Awards and Recognitions of the IEEE Portugal Section in 2014, He has been the Chair of the IEEE Portugal Joint Chapter on Antennas & Propagation—Electron Devices—Microwave Theory & Techniques since 2016 and a Regional Delegate of the European Association for Antennas and Propagation (EurAAP) for Andorra, Portugal, and Spain since March 2017. He is also an Associate Editor of the IEEE TRANSACTIONS ON ANTENNAS AND PROPAGATION and the *IET Microwaves, Antennas and Propagation*.

Arnaldo S. R. Oliveira (Member, IEEE) received the B.Sc. and M.Sc. degrees in electronics and telecommunications and the Ph.D. degree in electrical engineering from the University of Aveiro, Aveiro, Portugal, in 1997, 2000, and 2007, respectively.

He is currently a Researcher with the Telecommunications Institute, University of Aveiro, where he has been teaching computer architecture, digital systems design, programming languages, and embedded systems since 2001 and is currently an Assistant Professor. He participates in several national- and European-funded research projects. He is the author or a coauthor of more than 100 journal articles and international conference papers. His research interests include reconfigurable digital systems, software-defined radio, and next-generation radio access networks.

Nuno Borges de Carvalho (Fellow, IEEE) was born in Luanda, Angola, in 1972. He received the Diploma and Ph.D. degrees in electronics and telecommunications engineering from the University of Aveiro, Aveiro, Portugal, in 1995 and 2000, respectively.

He is currently a Full Professor and a Senior Research Scientist with the Institute of Telecommunications, University of Aveiro. He coauthored *Intermodulation in Microwave and Wireless Circuits* (Artech House, 2003), *Microwave and Wireless Measurement Techniques* (Cambridge University Press, 2013), and *White Space Communication Technologies* (Cambridge University Press, 2014). He holds six patents. His current research interests include software-defined radio front ends, wireless power transmission, nonlinear distortion analysis in microwave/wireless circuits and systems, measurement of nonlinear phenomena, and the design of dedicated radios and systems for newly emerging wireless technologies.

Dr. de Carvalho is also a member of the IEEE MTT AdCom. He was a recipient of the 1995 University of Aveiro and the Portuguese Engineering Association Prize for the Best 1995 Student at the University of Aveiro, the 1998 Student Paper Competition (Third Place) of the IEEE Microwave Theory and Techniques Society (IEEE MTT-S) of the International Microwave Symposium (IMS), and the 2000 IEEE Measurement Prize. He is a Distinguished Microwave Lecturer of the IEEE MTT-S. He is also the Past-Chair of the IEEE Portuguese Section, MTT-20, and MTT-11. He is also the Vice-Chair of the URSI Commission A (Metrology Group). He has served on the Technical Committees of MTT-24 and MTT-26. He has been a Reviewer and an author of over 200 articles in magazines and conferences. He is the Editor-in-Chief of the *Wireless Power Transfer* (Cambridge), an Associate Editor of the *IEEE Microwave Magazine*, and a former Associate Editor of the IEEE TRANSACTIONS ON MICROWAVE THEORY AND TECHNIQUES and the *Institution of Engineering and Technology* (*IET*) *Microwaves, Antennas and Propagation*.